

SELECTIVE EXHAUST GAS RECYCLING FOR CARBON CAPTURE APPLICATIONS: COMBUSTION AND OPERABILITY MEASUREMENT

R Marsh¹, A Giles¹, J Runyon¹, D Pugh¹, P Bowen¹, S Morris¹, A Valera-Medina¹, T Best², K Finney³, M Pourkashanian³.

¹Cardiff University, School of Engineering, CF24 3AA, UK

²Energy Technology & Innovation Initiative, Faculty of Engineering, University of Leeds, LS2 9JT, UK

³Energy 2050, Energy Engineering, Mechanical Engineering, University of Sheffield, S10 1TN, UK

Tel: +44 2920 876 852
marshr@cardiff.ac.uk

ABSTRACT

The use of exhaust gas recycling in gas turbine applications has been considered as a potential solution for low NO_x applications, but this concept is now gaining interest for intensification of CO₂ scrubbing for CCS applications (Evulet et al, 2009). Moreover, the idea of selectively recycling CO₂, rather than the entire exhaust gas is under consideration since it can potentially deliver a more compact engine / absorber configuration (Ali et al, 2014, 2016). This will involve some technical challenges that are addressed in the following paper, under the UK's EPSRC SELECT project.

Given that CO₂ acts as a heat sink, effectively reducing the flame temperature and burning rate in methane-air combustion, the study of highly quenched CO₂-doped flames has research potential in the development of industrial scale S-EGR power plants (Amato et al, 2011). In this paper a series of experiments is presented, demonstrating the behaviour of CO₂ quenched premixed swirl flames on an optical burner, followed by a small scale (50-80kWe) CHP gas turbine with CO₂ injection at the air inlet. Burner results demonstrated the effect of the CO₂ as a combustion inhibitor, causing downstream migration of the premixed flame zone, leading to eventual blow-off, instability and extinction, and necessitating a change in operation equivalence ratio. The influence that CO₂ has on produced CO and NO_x emission profiles is also presented, as functions of operational flame temperature.

NOMENCLATURE

AFT – Adiabatic Flame Temperature
CCS – Carbon Capture and Storage
DLE – Dry Low Emissions
EGR – Exhaust Gas Recycling
FWHM – Full Width at Half Maximum

GT – Gas Turbine

GTTC – Gas Turbine Research Centre

HPGSB – High-Pressure Generic Swirl Burner

HPOC – High Pressure Optical Chamber

PACT – Pilot-scale Advanced CO₂ Capture Technology

S-EGR – Selective Exhaust Gas Recycling

1. INTRODUCTION

EGR (originally for NO_x reduction in gas turbines) is receiving renewed interest as a potential strategy to intensify GT-CCS (Jansohn et al, 2011). Selective Exhaust Gas Recycling (S-EGR) has been suggested as a GT-CCS technique to improve CO₂ concentrations of the flue gas such that the cost and volume of the capture unit can be minimised (Merkel et al, 2013). This can potentially deliver process intensification and enhanced net cycle efficiency. In essence, the S-EGR concept recycles CO₂ enriched exhaust rather than exhaust gas only, therefore minimising the recycling of nitrogen within the EGR loop. Fig. 1 shows a process schematic of an S-EGR GT plant, indicating the selective CO₂ removal device (Belaissaoui et al, 2013) and the recycling loop.

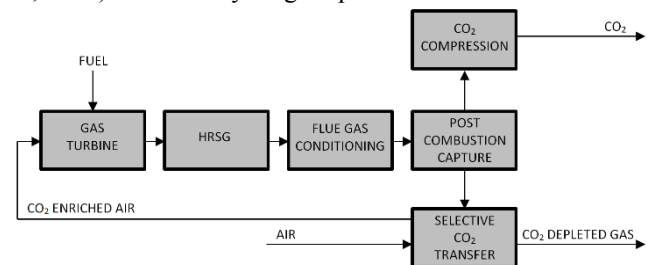


Fig. 1 Process schematic of a series configuration S-EGR system, including extraction points and recycling loops of pure CO₂ and depleted exhaust gas (Merkel et al, 2013).

At the time of writing, S-EGR has not been demonstrated on any meaningful scale and hence the aim of this research is to examine the behaviour of a modern premixed DLE swirl burner (Marsh et al, 2016) with high CO₂ concentrations in the inlet mixture (up to 20% molar).

2. METHODS

2.1 Optical Burner Experiments

The aim of the burner testing was to characterise the effect of CO₂ as a diluent, in terms of operational premixed CH₄/air flame stability, heat release, and measured exhaust gas composition. CO₂ has markedly higher density and heat capacity than air, and as a combustion diluent will reduce AFT, and hence overall reaction rate. The experiment was designed to provide scalable results, comparable with a modern DLE power generating gas turbine. Experimental conditions are summarised in Table 1, and were specified to maintain a constant total molar flow rate through the burner at a fixed inlet reactant temperature (573 K). The equivalence ratio (ϕ) was varied by reducing air supply for a corresponding increase in CO₂, thereby minimising changes in volumetric flow and burner nozzle outlet velocities in the turbulent flow field. Three bulk volumetric flow rates were specified in the stable operating regime; identified as low (LF), medium (MF), and high (HF). Changes in reactant density required molar fluxes to be increased in proportion with absolute pressure specification (1.1-2.2 bar_a), necessitating a rise in thermal power (42-84 kW) supplied to the burner and effectively holding the non-dimensional flow parameter, $\dot{m}\sqrt{T}/P$, constant.

Table 1. Experiment conditions examined for burner.

Condition	Air (g/s)	CO ₂ (g/s)	CH ₄ (g/s)	Pressure (bar _a)	Air + CO ₂ flow (mol/s)
42kW LF	17.1 – 14.9	2 - 5	0.84	1.1	0.64
42kW MF	21.5 – 18.8	1 - 5	0.84	1.1	0.77
42kW HF	26.1 – 24.8	0 - 2	0.84	1.1	0.90
84kW LF	30.6 – 28.6	9.1 - 12	1.68	2.2	1.27
84kW MF	39.1 – 35.6	8 - 13.1	1.68	2.2	1.54
84kW HF	52.2 – 49.4	0 – 4	1.68	2.2	1.81

The swirl burner was employed within the High Pressure Optical Chamber (HPOC) at Cardiff University's Gas Turbine Research Centre (GTRC) - with a schematic shown in Fig. 2. This burner is the second generation High-Pressure Generic Swirl Burner (HPGSB-2), which has a diametric expansion ratio of 2.5 to 1 from the burner nozzle exit, compared with 3.5 to 1 from the original HPGSB design. Reactants enter the burner inlet plenum (Fig. 2(a)) via fixed piping or flexible metallic hoses, with mass flows quantified using Coriolis meters (Emerson CMF010M, CMF025M CMF050M). Operational

conditions were monitored using an instrumentation lance (Fig. 2(b)) transmitting temperatures and rig dynamic pressure. The burner assembly is housed within the HPOC (Fig. 2(c)), rated to 1.6 MPa at 900 K. After entering the plenum, reactants travel through the premix chamber (Fig. 2(d)) to a single radial-tangential swirler (Fig. 2(e)) and out the burner exit nozzle (20 mm radius). The outlet has a geometric swirl number (Syred & Beer, 1974) equivalent to $S_g = 0.8$. Optical access is afforded via diametrically opposed quartz viewing windows (Fig. 2(f)), facilitating flame chemiluminescence measurement. The burner was operated with a 100 mm ID cylindrical quartz exhaust confinement tube (Fig. 2(g)). Air and CO₂ were mixed and preheated upstream, with the inlet plenum pre-conditioned, and held at 573±5 K. An N-Type thermocouple was employed downstream of the confinement exit to measure representative turbine entry temperatures. Pressure was maintained with proportional control of a remotely operated water-cooled back-pressure valve in the exhaust piping.

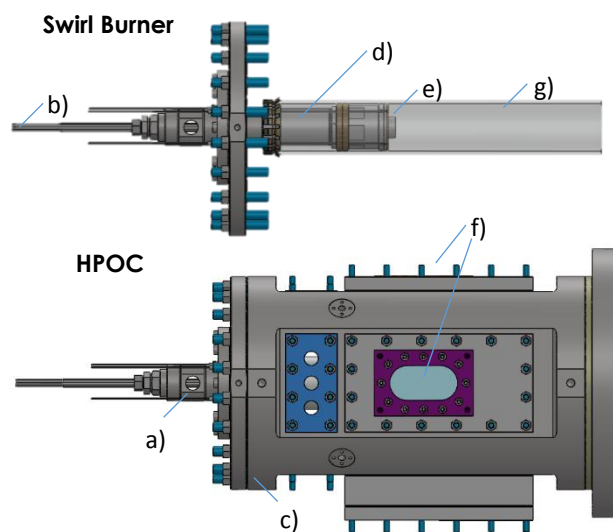


Fig. 2 Schematic view of the swirl burner employed with the HPOC, with components described in the text.

Exhaust gas sampling was undertaken at the exit of the quartz confinement; with the water-conditioned sample line maintained at 433K. Exhaust concentrations were quantified via an industry standard system supplied by Signal Gas Analysers Ltd. Measurements of O₂, CO₂, CO were taken dry (chilled to 275 K), with NO_x and unburnt hydrocarbons measured wet at 433 K to avoid absorption losses. The analysers have selectable ranges depending on the concentrations observed during the experiment. In this study there was potential for relatively large variations in the exhaust gas concentration, especially in CO₂ values. Calibration was undertaken using span gases in appropriate ranges, with certified gas compositions supplied by Air Products Ltd. Total uncertainty in each measurement was

on the order of ~5%, with the combined effects of analyser specification, span gas and linearisation.

Chemiluminescence, and in particular that produced by the thermally-excited state of the hydroxyl radical (OH^*), has been utilised in this work as a qualitative indication of localised heat release within the swirl flame interrogation area. The chemiluminescence image capture system utilises a bandpass filtered ($315 \text{ nm} \pm 15 \text{ nm}$ FWHM) intensified CCD camera and has been detailed in previous works (Runyon et al, 2015). Each image is 1024×1344 pixels in the axial and radial directions, respectively, with a resolution of 13.6 pixels/mm yielding a field of view of approximately $75 \text{ mm} \times 100 \text{ mm}$, centred at the burner nozzle exit. Thus, in proceeding images, $r = 0 \text{ mm}$ represents the burner exit nozzle centreline and $y = 0 \text{ mm}$ represents the edge of the burner exit nozzle. Given the high CO_2 dilution levels studied in this work, the gate timing of the image intensifier was set at $400 \mu\text{s}$ while the gain was held constant throughout all test conditions to ensure comparability while optimizing the signal to noise ratio. At each experimental condition, 200 images were captured at a rate of 10 Hz. In order to process these images for presentation, instantaneous images in each data set were filtered using a 2-D adaptive noise-removal filter and then temporally averaged and corrected for background intensity. A modified, open source Abel inversion algorithm (Killer, 2014) was then utilised to project the line-of-sight integrated chemiluminescence intensity distribution onto a theoretical 2-D focal plane. This procedure enhances the discrete areas of heat release within the image, assuming that the swirl flame is axisymmetric about the burner centreline ($r = 0 \text{ mm}$). Finally, for further comparison between OH^* intensity levels under varying rig operating conditions, an integral intensity was utilised, defined in Eq. 1 as a pixel-wise summation of the OH^* intensity values from the temporally averaged and background corrected OH^* chemiluminescence images.

$$I_{\text{OH}^*} = \sum_{i=1}^{1344} \sum_{j=1}^{1024} \bar{I}_{\text{OH}^*_{i,j}} \quad (1)$$

A false colourmap directly correlated to the pixel signal intensity of the original black and white image was applied to provide visual representation of the location of the highest concentrations of OH^* radicals in the reaction zone, and thus indication of the flame front location and localised heat release.

2.2 Selective EGR simulation in Turbec T100 engine via CO_2 injection.

The aim of the engine test was to compare the premixed burner experiment on a similar burner scale, but within an actual engine subject to an electrical load. Therefore, a parallel activity in this research involved the demonstration of a small-scale gas turbine unit. The

purpose of using the results from the engine test in this paper is to demonstrate an engine system-based approach, rather than idealised conditions within an optical combustion rig. A Series 1 Turbec T100 PH micro gas turbine generator system (located at the UKCCSRC PACT Core Facilities) was used, modified for CO_2 injection into the compressor inlet. The engine generates up to 100 kW of electrical power – at high efficiency with low emissions – and up to 165 kW of heat in the form of hot water. The engine has a lean, pre-mixed combustor, similar in size and configuration to the swirl burner used for the research in this paper. The key difference between the two systems is the standard practice of adding staged dilution air around the combustion chamber of the engine (De Santis et al, 2016), whereas in the HPOC a non-diluted quartz confinement is used. More detailed information regarding the setup, test conditions and results are presented in Best et al (2016).

3. RESULTS

3.1 Burner Results

Figs. 3 and 4 show the achievable equivalence ratios at each molar flow rate (HF to LF, left to right) for the 1.1 and 2.2 bar_a experiments (42 and 84 kW) in relation to CO_2 addition. The three data series in each figure therefore span the supply rates, defined in Table 1 as the stable ranges over which the flame could be maintained. Excessive CO_2 addition at the leanest conditions led to a reduction in AFT and burning rate, resulting in flame instability, blow-off and extinction. Moreover, CO_2 dilution was necessary at near stoichiometric conditions with the lowest flow rates to avoid premixed flashback, defined here by high temperatures ($>1300 \text{ K}$) at the tip of the instrumentation lance located as a bluff body upstream of the burner nozzle exit. An increase in pressure is shown to provide a further reduction in burning rate, and thereby narrows the stable operating range while shifting it towards higher equivalence ratios.

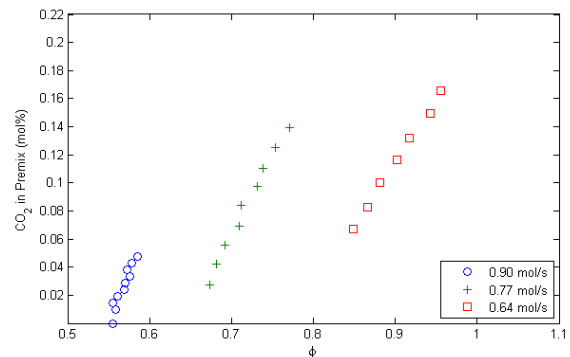


Fig. 3 Stable operating conditions shown as CO_2 molar concentration vs equivalence ratio of the blend at 1.1 bar_a and 42 kW.

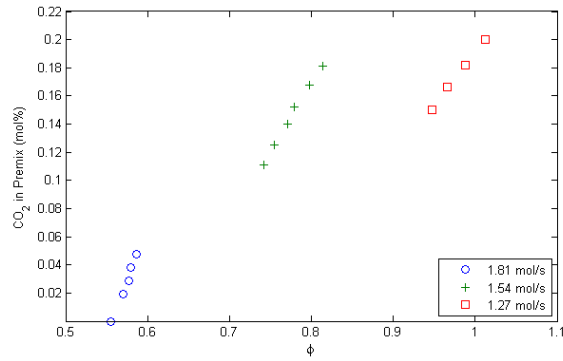


Fig. 4 Stable operating conditions, shown as CO₂ molar concentration vs equivalence ratio of the blend at 2.2 bar_a and 84 kW.

Figs. 5 and 6 show the Abel deconvoluted OH* chemiluminescence images of the burner experiments at 42 kW, for respective molar flow rates of 0.9 and 0.64 mol/s. Each series of images is at constant molar flow rate with increasing CO₂ concentration in the oxidant. The effect of CO₂ can clearly be seen to result in downstream migration of the flame in the consistent flow field, coupled with a spreading and weakening of the heat release zone. This can again be attributed to the reduction in AFT, and resulting burning rate for the addition of diluent CO₂. This correlates with the reduction in stable operating ranges shown in Figs. 3 and 4.

In Fig. 5 (0.9 mol/s), the three images clearly show that with increasing CO₂ flow, the heat release zone has extended with OH* intensities shifting further downstream in the flow, and enhanced outer recirculation zones. In the top image, representative of a CH₄-air flame (0% CO₂ addition), the heat release zone (and thus presumed flame location) lies along the outward expanding shear layer. The 2-D planar representation of the 3-D conical flame shape typical of swirl-stabilised combustion therefore yields a V-shaped flame pattern. As the CO₂ concentration increases and the reaction progress slows, the flame migrates downstream and is influenced by the outer recirculation zone and impingement on the confinement walls, yielding a more M-shaped flame. Comparing the high net molar flux to the 0.64 mol/s case shown in Fig. 6, the flame is shortened with the reduction in bulk flow. Significantly higher CO₂ concentrations were reached at the lower molar flux due to the higher reactivity of the employed equivalence ratio. As shown in Fig. 3, a near stoichiometric ratio was achieved at 16.6% CO₂ addition, although in Fig. 6 the flame is shown to be weakening at this condition. The reduction in bulk flow coupled with higher reactivity results in a compact flame shape which moves upstream towards the burner nozzle exit with a reduction in CO₂ flow. This potential for flashback means that a comparable CH₄-air (0% CO₂ addition) flame could not be maintained in the burner at the LF and MF molar flow rates.

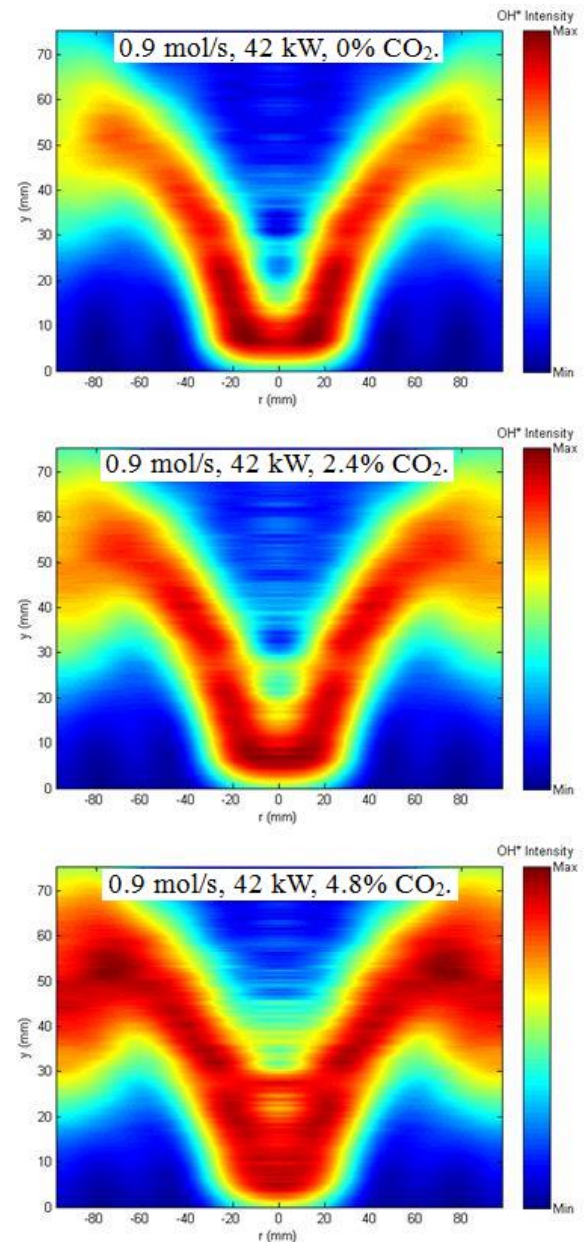


Fig. 5 Abel inverted chemiluminescence images at 42 kW, 1.1 bar_a and 0.9 mol/s total flow for three CO₂ concentrations in the inlet premix.

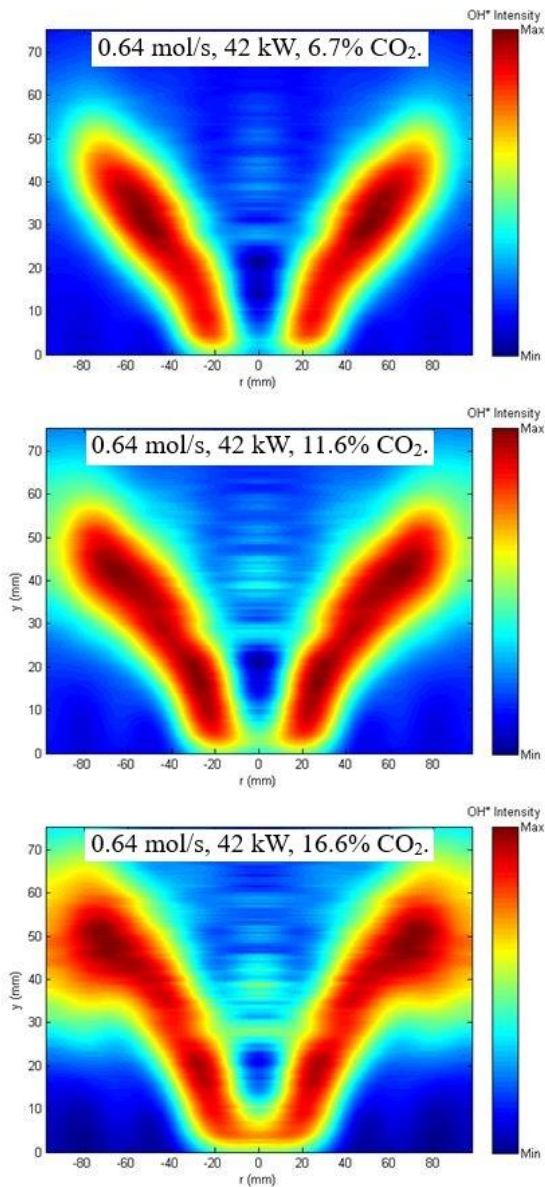


Fig. 6 Abel inverted chemiluminescence images at 42 kW, 1.1 bar_a and 0.64 mol/s total flow for three CO₂ concentrations in the inlet premix.

At the higher operating power and pressure, Figs. 7 and 8 show a similar trend for CO₂ addition with downstream migration of heat release and expanded outer recirculation zones. It should be emphasised that the total molar flow rate has doubled between the two operating conditions, but bulk flow velocity should be approximately maintained due to the change in reactant density. Consequently, the effect on the flow-field was minimal - hence why there are only minor differences in heat release profiles for changes in pressure between Figs. 5 and 7, together with the 16.6% CO₂ cases at 0.64 and 1.27 mol/s. Higher CO₂ concentrations were achieved for the LF conditions at 84 kW, attributed to the higher overall operational equivalence ratio, and a relative reduction in local heat

loss. The latter influence was supported by the measured burner face and exhaust temperatures, which were on the order of ~100 K higher at 84 kW for near identical equivalence ratios and levels of CO₂ addition.

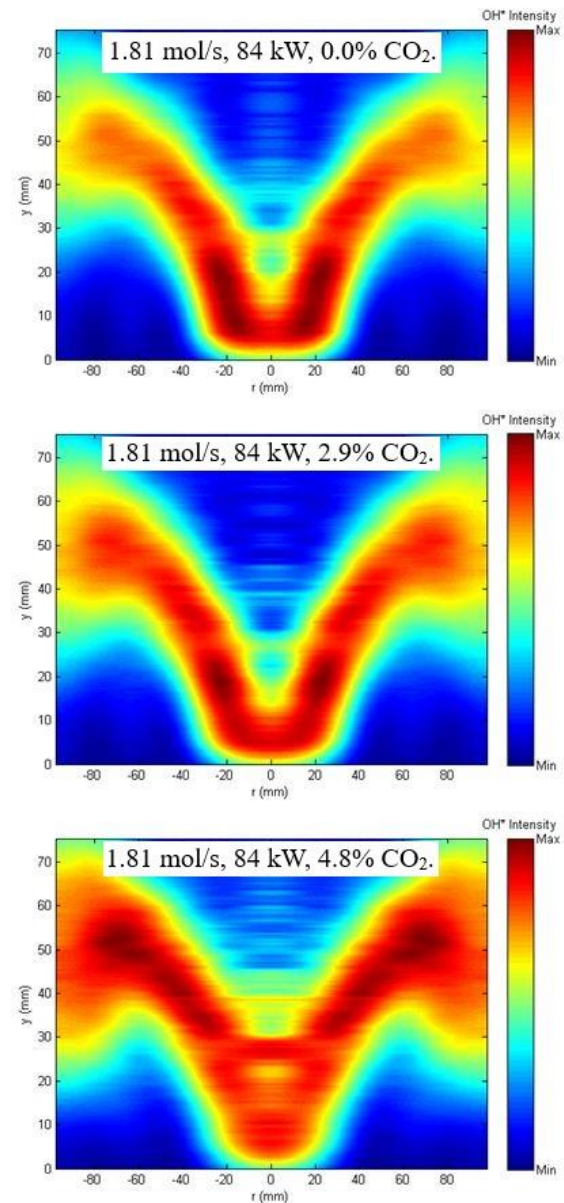


Fig. 7 Abel inverted chemiluminescence images at 84 kW, 2.2 bar_a and 1.81 mol/s total flow for three CO₂ concentrations in the inlet premix.

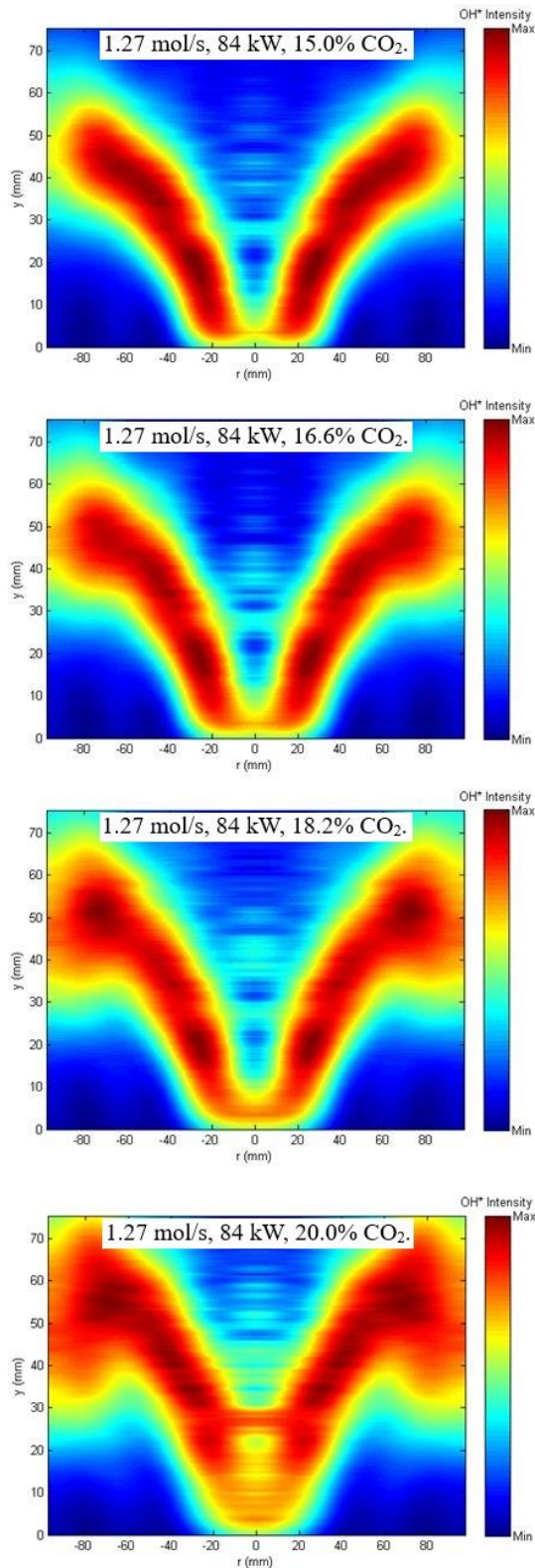


Fig. 8 Abel inverted chemiluminescence images at 84 kW, 2.2 bar_a and 1.27 mol/s total flow for four CO₂ concentrations in the inlet premix.

Figs. 9 and 10 show the respective 42 kW and 84 kW average chemiluminescence image intensities for all experimental conditions (corresponding to the 41 data points shown in Figs. 3 and 4). The effect of increasing CO₂ concentration was consistently shown to reduce the overall averaged intensity, and hence heat release, with highest values corresponding to the highest equivalence ratio, and hence hottest conditions. In comparison to typical CH₄-air flames, in which the OH* chemiluminescence intensity has been shown to increase with increasing equivalence ratio to near stoichiometry and then drop thereafter (Runyon et al, 2015), the CO₂-diluted flame shows the same trend generally with decreasing molar flow rate. However, at a fixed molar flow rate, the OH* chemiluminescence intensity is shown to decrease with increasing equivalence ratio due to the change in heat capacity between N₂ and CO₂ as combustion diluents.

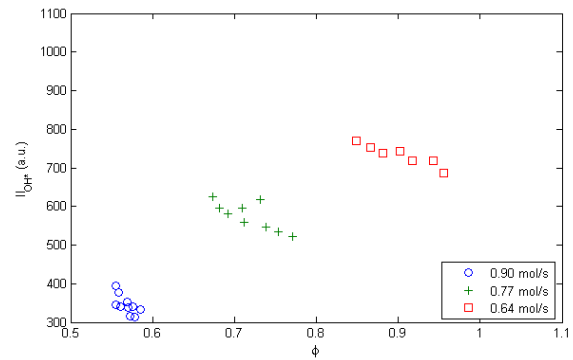


Fig. 9 Average image chemiluminescence intensities for each flow and CO₂ condition at 42 kW, 1.1 bar_a.

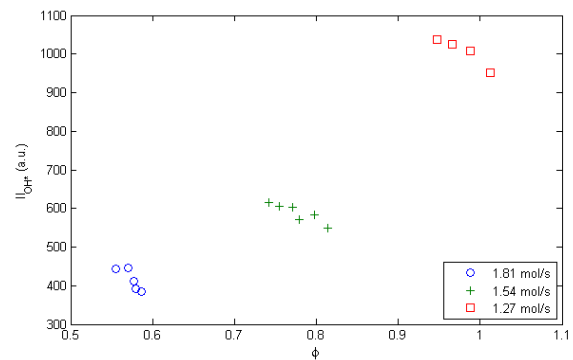


Fig. 10 Average image chemiluminescence intensities for each flow and CO₂ condition at 84 kW, 2.2 bar_a.

Figs. 11 and 12 show the effect of CO₂ addition on CO concentration in the exhaust products at the respective 1.1 bar_a and 2.2 bar_a conditions. Also included on each of the plots are AFT values, modelled using a constant pressure equilibrium reactor on CHEMKIN-PRO (GRI-Mech 3.0 reaction mechanism was used, employing 53 species and 325 reactions) with each of the logged mass flow values.

Thus, the open symbols (AFT) correspond directly to the closed symbols (CO) at each CO₂ concentration point (it should be noted that one 1.27 mol/s condition in Fig. 12 has been omitted, as this point was near $\phi=1$ where CO production was increased above the maximum scale for the analyser). The effect of adding CO₂ was identical and repeatable for each molar flow rate and power combination - an expected reduction in AFT, coupled with an increase in measured CO concentration. However, if equivalent CO₂ loadings are compared (where datasets overlap on the horizontal axis) between different flow conditions (and hence ϕ value), higher CO readings are measured for a step increase in AFT, driven by incomplete combustion (Marsh et al, 2016). This suggests a trade-off; where increases in both AFT and CO₂ will drive a rise in CO, however an increase in the latter will inherently cool the flame and therefore partially reduce potential CO formation at a fixed molar flowrate. Results therefore suggest that cooler, leaner operation is required to minimise CO production for the increased addition of CO₂. Moreover, an increase in pressure was shown to reduce equivalent CO concentrations between the two datasets.

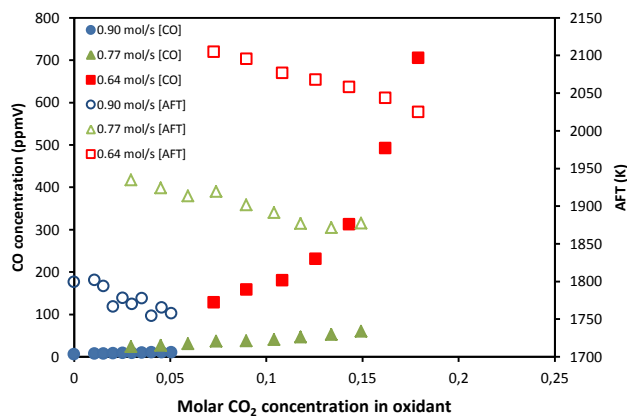


Fig. 11 Measured CO concentrations and modelled AFT for each flow and CO₂ condition at 42 kW, 1.1 bar_a.

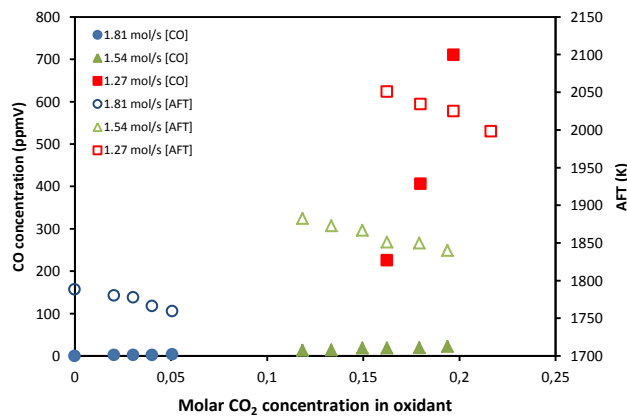


Fig. 12 Measured CO concentrations and modelled AFT for each flow and CO₂ condition at 84 kW, 2.2 bar_a.

Therefore, high levels of CO₂ dilution from these results clearly produce unacceptably high quantities of CO for most of the employed experimental conditions. This is in agreement to similar work by Yu et al (2013). Further work must be undertaken to optimise operational equivalence ratios with CO₂ loading against CO concentrations, to maximise the potential effectiveness of CO₂ capture processes.

Normalised (dry, 15% O₂) NO_x concentrations are plotted against CO₂ loading in Figs. 13 and 14, for the respective 1.1 and 2.2 bar_a conditions. CO₂ addition is shown to reduce NO_x production for all conditions tested, with the plotted profiles demonstrating a similar relationship to AFT. This suggests that thermal NO_x production is dominant (as would be expected with CH₄-air combustion) and again cooler, leaner conditions provide the lowest concentrations. A comparison of equivalent CO₂ loadings between Figs. 13 and 14 shows the influence of pressure on NO_x production is small, with a marginal increase at 2.2 bar_a and 84kW.

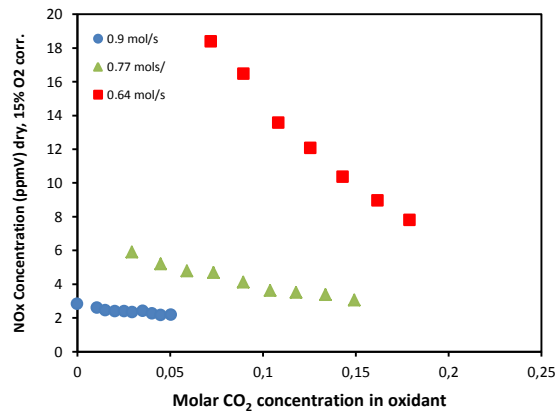


Fig. 13 Normalised (dry 15%O₂) NO_x concentrations for each flow and CO₂ condition at 42 kW, 1.1 bar_a.

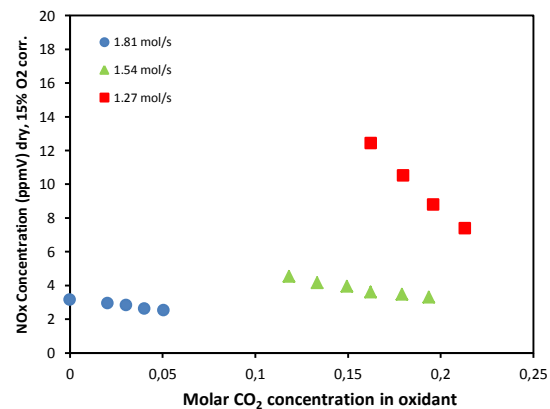


Fig. 14 Normalised (dry 15%O₂) NO_x concentrations for each flow and CO₂ condition at 84 kW, 2.2 bar_a.

2.2 Selective EGR simulation in Turbec T100 engine via CO₂ injection.

The results from the engine test are shown in Table 2, which include CO and NO_x emissions as a function of the engine power setting. These include two values per power; (1) zero injected CO₂ and (2) at the maximum CO₂ flowrate of 125 kg/hr (34.7 g/s) through the engine. 50 kW represents the minimum stable turndown for this engine and thus at 34.7 g/s flow rate the maximum CO₂ concentration in the inlet is achieved. It should be noted that when the engine power is reduced to minimum turndown at 50 kW, the nominal (0 g/s CO₂) CO concentrations increase as the flame weakens, but the effect of CO₂ dilution is significantly more pronounced at these low power settings. This is in close agreement with the burner tests in the previous section, illustrating that the CO₂ has a marked effect on flame chemistry at high concentrations for the reasons outlined above.

The values of NO_x appear largely unaffected by CO₂ injection, which is logical given the lean-burn and high dilution arrangement of the T100 (De Santis et al, 2016) whereas in the burner experiments there is no additional dilution downstream of the burner, and hence the relationship between CO₂ dilution and NO_x is more pronounced.

Table 2. Gas analysis results for the nominal and CO₂ diluted conditions in the Turbec T100 engine.

Power (kW)	CO (ppmV dry)		NO _x (ppmV dry)	
	0 g/s CO ₂	34.7 g/s CO ₂	0 g/s CO ₂	34.7 g/s CO ₂
50	22.0	143.0	1.6	1.4
55	4.3	52.0	-	-
60	2.2	4.9	1.3	0.6
65	2.0	0.1	-	-
70	1.8	3.8	1.3	0.8
75	0.4	0.0	-	-
80	0.0	0.0	1.4	1.1

CONCLUSIONS

- The influence of CO₂ addition was investigated on a premixed CH₄/air flame, scaled for practical relevance in a representative gas turbine swirl burner at two separate pressure (1.1-2.2 bar_a) and power (42-84 kW) conditions. The increased addition of CO₂ necessitated a change in stable operating equivalence ratio. The largest quantities (~20%mol) of CO₂ required near stoichiometric air-fuel ratios, otherwise unachievable due to potential for premixed flashback.

- Bulk flow profiles were maintained at disparate molar conditions, with flame heat release analysed using OH* chemiluminescence imaging. An increase in CO₂ concentration was shown to promote downstream migration on the flame and thickening of the heat release profile, as adiabatic flame temperature and burning rate were reduced. Further increases in CO₂ addition would lead to eventual flame blowoff, instability and extinction, necessitating the change in equivalence ratio for stable operation.
- Increase in CO₂ addition, together with the necessary enhancement in equivalence ratio, both led to a rise in exhaust CO concentrations. The quantities measured may be significantly detrimental to downstream CO₂ capture processes, and therefore operational conditions must be carefully specified and controlled. The efficiency of the capture process may be optimised with regard to operational equivalence ratio, CO₂ loading, and CO emissions. NO_x emissions were also shown to be reduced for the addition of CO₂ with leaner combustion, as thermal production pathways are quenched at cooler temperatures.
- In the T100 engine test the results agree with the burner experiments for CO production, in that high concentrations of CO₂ cool the flame and result in high CO levels. There was no agreement in terms of NO_x concentrations although this has been attributed to the high secondary dilution in the engine (and thus low NO_x levels), not present in the HPOC configuration.

ACKNOWLEDGEMENTS

The work was funded by EPSRC SELECT grant EP/M001482/1, and EPSRC Gas-FACTS: Gas – Future Advanced Capture Technology Options, EP/J020788/1. Work undertaken at the Cardiff University’s Gas Turbine Research Centre (GTRC) was with invaluable technical support from Jack Thomas and Terry Treherne. The authors would also like to acknowledge the UKCCSRC for making the PACT Core Facilities available for the research.

References

U Ali, T Best, K Finney, C Font Palma, K Hughes, D Ingham, M Pourkashanian. Process Simulation and Thermodynamic Analysis of a Micro Turbine with Post-combustion CO₂ Capture and Exhaust Gas Recirculation Energy Procedia, 63, (2014) 986-996.

- U Ali, E Agbonghae, K Hughes, D Ingham, L Ma, M Pourkashanian. 'Techno-economic process design of a commercial-scale amine-based CO₂ capture system for natural gas combined cycle power plant with exhaust gas recirculation.' *Applied Thermal Engineering* (2016) 103, 747–758.
- A Amato, B Hudak, P D'Carlo, D Noble, D Scarborough, J Seitzman, T Lieuwen. Methane Oxycombustion for low CO₂ cycles: Blowoff Measurements and Analysis. *Journal of Engineering for Gas Turbines and Power* 133 (2011).
- B Belaïssaoui, G Cabot, M Cabot, D Willson, E Favre. CO₂ capture for gas turbines: an integrated energy-efficient process combining combustion in oxygen-enriched air, flue gas recirculation, and membrane separation. *Chemical Engineering Science*, 97, (2013) 256-263.
- T Best, K Finney, A De Santis, D Ingham, M Pourkashanian. Exhaust gas recirculation and selective exhaust gas recirculation on a micro gas turbine for enhanced CO₂ capture performance. 8th International Gas Turbine Conference (2016) European Turbine Network.
- A De Santis, D Ingham, L Ma, M Pourkashanian. CFD analysis of exhaust gas recirculation in a micro gas turbine combustor for CO₂ capture. *Fuel*, Volume 173, (2016) 146-154.
- A Evulet, A Elkady, A Brand, D Chinn On the performance and operability of GE's low NO_x combustors utilising exhaust gas recirculation for post combustion carbon capture. *Energy Procedia* 1. (2009) 3809-3816.
- GRI-Mech3.0 <<http://www.me.berkeley.edu/gri-mech/>>; 2015 Accessed 01/12/2015.
- P Jansohn, T Griffin, I Mantzaras, F Marechal, F Clemens. Technologies for gas turbine power generation with CO₂ mitigation *Energy Procedia*, 4 (2011) 1901-1908.
- Killer, C. 2014. Abel Inversion Algorithm, MATLAB Central File Exchange, <http://www.mathworks.com/matlabcentral/fileexchange/43639-abel-inversion-algorithm>
- R. Marsh, J. Runyon, A. Giles, S. Morris, D. Pugh, A. Valera-Medina, P. Bowen. Premixed methane oxycombustion in nitrogen and carbon dioxide atmospheres: measurement of operating limits, flame location and emissions. *Proceedings of the Combustion Institute*, 36 (2016), in press.
- T Merkel, X Wei, Z He, L White, J Wijmans, R Baker. Selective Exhaust Gas Recycle with Membranes for CO₂ Capture from Natural Gas Combined Cycle Power Plants. *Industrial Energy and Chemistry Research*. (2013) 52, 1150–1159.
- Runyon, J. et al. 2015. *Proceedings of the 7th European Combustion Meeting* (2015) 3-29.
- N Syred. & J Beer. *Combustion in Swirling Flows: A Review*. *Combustion and Flame*, 1974, 23, 143-201.
- B Yu, S Kum, C Lee, S Lee. 'Effects of exhaust gas recirculation on the thermal efficiency and combustion characteristics for premixed combustion system.' *Energy*, 49 (2013) 375-383.